Thermoacoustic enrichment of the isotopes of neon

D. A. Geller and G. W. Swift
Condensed Matter and Thermal Physics Group, Los Alamos National Laboratory, Los Alamos, New Mexico 87545

(Received 30 October 2003; accepted for publication 28 January 2004)

The enrichment of the neon isotopes in a thermoacoustic device is demonstrated. Because the thermal diffusion ratio of neon is small, an apparatus longer than a wavelength was necessary in order to easily observe the separation. The device was modular and extensible, so that arbitrarily large separations could in principle be obtained. The acoustic duct was a series of multiple, identical quarter-wavelength modules with side-branch drivers. In this way, waveforms close to that of a traveling wave were maintained in the duct, despite the high acoustic attenuation caused by the duct's small diameter and large length. The concentrations of the isotopes were measured at one end of the duct using a quadrupole mass spectrometer. For the operating frequency of 227 Hz, the maximum separation gradient obtained was 0.43%/m, and mole fluxes at zero gradient as high as 3 nmol/s were observed. Effects of turbulence, though not observed, are also discussed, and the scaling properties of this method are compared with those of traditional mixture-separation methods. © *2004 Acoustical Society of America.* [DOI: 10.1121/1.1687831]

PACS numbers: 43.35.Ud, 43.20.Mv, 43.35.Ty [RR] Pages: 2059–2070

I. INTRODUCTION

Material separation is one of the central challenges of chemical engineering and related industries, and the development of separation techniques remains an active field of research today.[1] Because of the wide range of applications for separation, no single technique addresses all possible needs. Distillation is most widely used because it is, in principle, thermodynamically reversible and therefore offers very high energy efficiency. However, when separating mixtures for which the difference in vapor pressures is small or zero, as in isotope or azeotrope separations, or in cases where distillation would require extremely high or low temperatures or pressures, other techniques can become competitive. Because the capital cost of a distillation device is high for such challenging separations, other methods may be particularly attractive when only small amounts of material are to be processed. The crossover depends on where the cost of a distillation plant becomes comparable to the energy cost of these inefficient methods.

The physical basis for a new separation method based on thermoacoustics was described in several recent articles.[2–5] The thermoacoustic separation process depends on thermal diffusion and viscosity in a binary mixture to produce time-averaged mass fluxes of the mixture's two components in opposite directions. Because both diffusion and viscosity are dissipative, thermoacoustic separation has a low thermodynamic efficiency, on the order of that of conventional thermal diffusion or gaseous diffusion. However, thermoacoustic separation has potential advantages due to its mechanical simplicity and the promise of separation machines quite compact in size.

In this paper, we describe how one can apply the thermoacoustic separation technique in a practical configuration.[6] As a concrete example, we focus on enrichment of the neon isotopes, starting with a sample in which the isotopes are present in their natural abundances. This choice is partly made in deference to history: The first[7] isotope separation by gaseous diffusion was that of neon in 1920, and one of the earliest isotope separations by conventional thermal diffusion was that of neon in 1938 by Clusius and Dickel.[8]

Neon is also a logical choice for this exploration of thermoacoustic isotope enrichment because it is one of the easiest gaseous isotopic systems to separate. The mass difference between the predominant isotopes, ^{20}Ne and ^{22}Ne, is a high fraction of the average mass of the isotopes, resulting in a comparatively large thermal diffusion coefficient. Furthermore, the two predominant isotopes are naturally present[9] in concentrations of about 90.51% (^{20}Ne) and 9.22% (^{22}Ne), more nearly equal than those of other natural binary isotopic mixtures. Thus, no enrichment or preparation of the gas sample was necessary prior to our experiments in order to ensure measurable quantities of both isotopes. Nevertheless, 91–9 ^{20}Ne–^{22}Ne is considerably more challenging[10] to separate than the 50–50 He–Ar mixtures of previous, proof-of-principle experiments,[3,4] because the thermal diffusion ratio is about 50 times smaller.

In the following sections we describe how one can concatenate several modules similar to the experimental device described in Refs. 3 and 4 to separate gas mixtures to a desired degree. A first variation of the method uses a quasi-traveling wave. We outline how one goes about the basic design of such a thermoacoustic separator, we review how one properly quantifies the degree of separation of such a device and each of its modules, and we present an expression relating the number of modules to the separation one can achieve. We then describe an experiment demonstrating neon isotope enrichment by such an extended device, and we compare its measured performance with our calculated expectations. A second variant of the method produces an acoustic impedance higher than that of a traveling wave at equally spaced locations along the duct. Experiments confirm the

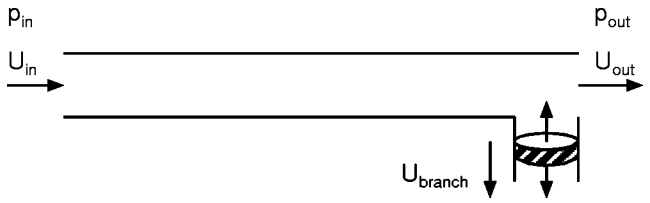

FIG. 1. Assembling a large enough number of modules like this one in series creates a thermoacoustic mixture separator capable of reaching any desired purities.

expected behavior of this variant and demonstrate its modest advantages. The Appendix lists definitions of variables and the results from previous work that are used here.

II. EXTENDING THE SYSTEM

In the experiments[3,4] on He–Ar, the concentrations of the two species could differ by as much as 10% along the tube length of $\sim 1/40$ of a wavelength. For isotopes, the thermal diffusion ratios are generally small so that, to achieve the same degree of separation, either a proportionally longer tube is necessary or one must process the gas in many batches. In the case of laboratory-scale purifications, batch processing of the gas might be reasonable if the number of batch steps is small. However, if the mixture to be processed is so expensive that one cannot simply discard the tailings at the end of each step, then recovery from the tailings requires additional steps and a complex inventory control for the products of each batch. Such batch-mode processing is difficult and tedious.

Hence, thermoacoustic separation in ducts of length greater than a wavelength is advantageous. The method we consider for doing this is to maintain an essentially traveling wave in a duct of arbitrarily great length by providing identical active branches at equally spaced distances along the duct, driven with time phasings appropriate to maintain the amplitude of the wave. Thus, the pressure and volume velocity[11] oscillations at each point between two adjacent drive branches are equal in amplitude but time shifted from the pressure and volume velocity oscillations at the corresponding point between any other pair of adjacent side branches. This is somewhat similar in concept to the ''acoustitron'' of Ref. 12, except that our topology has two ends, comprising a source and a sink for the traveling wave. Were there only one acoustic driver in the system, then the amplitude of the sound wave would decay as the wave traveled along the duct. In our realization of the system, the unit module from which the acoustic network is constructed consists of a length of duct with a tee at one end, one side of the tee leading through a short duct to a sealed bellows, as depicted in Fig. 1. Each bellows is driven lengthwise like a piston by the voice coil of an electrodynamic speaker. At the ends of the concatenation of identical unit modules are similar ducts with similarly driven bellows, one of which starts the wave traveling along the duct while the other actively absorbs it.

The most convenient realization of this scheme has each module one-quarter wavelength long and adjacent speakers phased $-90°$ from one another in time along the duct. This is a practical design because it allows all branches in the acoustic network to be driven with only two electrical signals in quadrature, rather than a larger number of equally spaced signal phasings. This significantly simplifies the electronics needed to drive the array of speakers.

For nonzero spacing between branches, there is always some variation in the amplitudes of pressure and volume velocity as a function of distance along any single module, because of the viscous and thermal attenuations.[5] In addition, the pressure and volume velocity do not have a constant time-phase difference along the duct. As a result, the limiting concentration gradient varies somewhat along the duct. For the oscillating pressure, the boundary condition required on each module is that the amplitude is the same at the beginning and end of the module. The amplitude of volume velocity must also be the same at the beginning and end of the module, but the presence of the branch means that this equality is achieved by adding the volume velocity from the branch to the volume velocity at the end of the duct, with appropriate time phasing. The volume velocity just before the branch is lower than that at the beginning of the duct because of the attenuation along the duct. One result of these two boundary conditions on pressure and volume velocity is that the highest limiting concentration gradient limiting appears near the end of the module just before the branch.

III. DETERMINING THE NUMBER OF MODULES

Before setting out to engineer the acoustics of a thermoacoustic separator, one must assess the kind of performance it will provide. Equations (25) and (36) from Ref. 5, reproduced here in the Appendix, show that the maximum concentration gradient and the maximum efficiency for thermoacoustic separation decrease quickly as the mole fractions of the two components in the binary mixture approach zero and unity, both through their explicit dependence on mole fractions and indirectly through their dependence on the thermal diffusion ratio k_T. The thermal diffusion ratio is approximately proportional to $n(1-n)$, where n is the mole fraction of the component of greatest interest. It is therefore natural to ask whether thermoacoustic separation can ever produce high-purity gases and whether it is at a severe disadvantage in doing so compared to other separation methods. In the case of Eq. (25) in Ref. 5, the factor of k_T implies that the maximum concentration gradient achievable for the desired component falls off approximately[13] as $(1-n)$; this would appear to offer diminishing returns as the enriched gas is further purified. It is more useful, however, to evaluate the separation in terms of the ''separation factor,'' defined in mixture-separation engineering[14] as the ratio of the relative abundances at the beginning and the end of one batch or one stage of processing

$$q=\frac{n_f/(1-n_f)}{n_i/(1-n_i)}, \tag{1}$$

where the subscripts i and f denote initial and final, respectively. For a stepwise separation process, like fractional distillation or gaseous diffusion, q typically turns out to be nearly the same for all steps.[14,15] If several steps are concat-

enated, the total separation factor of the apparatus is equal to the product of the q_j for each step j. For thermoacoustic separation, there are no clearly defined steps, but we may divide the separation duct of total length ℓ into pieces of length Δx. Considering each piece to be a separation step allowed to run to saturation, we can compute the separation factor for the jth piece to be

$$q_j = 1 + \frac{1}{n(1-n)}\left(\frac{dn}{dx}\right)_{\lim} \Delta x. \tag{2}$$

Because most of the n dependence in the expression for the limiting gradient $(dn/dx)_{\lim}$ derives from the factor k_T, q_j is nearly independent of concentration.[13]

In the limit that the duct is subdivided into infinitesimal pieces, we can write for the total separation factor of the duct

$$q_{\text{tot}} = \lim_{\Delta x \to 0} \prod_j q_j = \exp\left[\frac{1}{n(1-n)}\left(\frac{dn}{dx}\right)_{\lim} \ell\right], \tag{3}$$

where n and $(dn/dx)_{\lim}$ are evaluated at any point along the duct. As the duct is lengthened, q_{tot} approaches either 0 or ∞ depending on the sign of $(dn/dx)_{\lim}$, and this corresponds to concentrations n approaching 0 or 1, respectively. Purification of mixed gases thus improves exponentially with the length of the thermoacoustic device, just as it does with the number of stages in distillation or gaseous diffusion plants.

The peak thermodynamic efficiency of thermoacoustic separation is seen from Eq. (36) of Ref. 5 to be approximately proportional to $n(1-n)$, so that it also declines in proportion to the depleted component's concentration. In order to compare methods, it is simplest to consider how much energy must be expended to achieve a given total separation factor q_{tot}. For thermoacoustic separation, the acoustic power needed to obtain a factor q_j is proportional to the length of the duct. As extra lengths of duct are added in order to provide extra factors of q_j, the dissipation will increase linearly with the length. Thermal, viscous, and radiative losses in a Clusius–Dickel column also scale with the length of the column. For a gaseous diffusion plant, mechanical work is lost by free expansion and viscosity at each stage of the plant, so that the free energy dissipated is again proportional to the number of stages with separation factor q_j. Distillation is reversible in principle, but in practice free energy is lost due to pressure drops across the column which are proportional to the number of distillation plates or stages. Cryogenic distillation also suffers from heat leaks which scale as the length of the column. So, even for this ideally reversible process, the losses scale approximately as the number of factors of q_j.

Hence, both for separation factor and for energy efficiency, at high purities the scaling behavior of thermoacoustic mixture separation is the same as that of other mixture-separation systems.

IV. HARDWARE DESIGN CONSIDERATIONS

For this experiment, we developed a $|z| \approx \rho a$ system—a ''nearly traveling-wave system''—to study the separation of neon isotopes starting from a sample of pure neon with natural isotopic abundances. In our notation, z is the complex specific acoustic impedance Ap_1/U_1, ρ is the density of the gas, a is its speed of sound, p_1 is the complex oscillating pressure, U_1 is the complex oscillating volume velocity,[11] and A is the cross-sectional area of the duct. In the experiment, we anticipated needing a change in concentration of each isotope of about 1% across the duct in order that the separation effect be clearly measurable. From Eq. (25) in Ref. 5, reproduced here in the Appendix, it is straightforward to show that

$$\left(\frac{dn}{dx}\right)_{\lim} \approx (\gamma - 1)\frac{2\pi}{\lambda} k_T, \tag{4}$$

for the $|z| \approx \rho a$ system in the boundary-layer limit, where γ is the ratio of the isobaric to the isochoric specific heats and λ is the wavelength. To obtain this expression, we have used the fact that the waves are nearly traveling waves and that F_{trav} and F_{grad} (defined in Ref. 4 and in the Appendix) are of the same order in magnitude, and we have assumed that the amplitude of the sound is high enough that the steady axial diffusion does not appreciably limit the concentration gradient. For monatomic gases like neon, $\gamma = 5/3$. Furthermore, if k_T is small enough that the concentrations of the gas species do not change substantially (i.e., $\Delta n \ll n$) over the span of a single quarter-wavelength module, then k_T itself changes little between the ends of the module. Thus, we can avoid use of Eq. (3) from the previous section and write the separation across a single module as $\Delta n \approx (\gamma - 1)(\pi/2)k_T$. For neon with natural isotopic abundances,[16] $k_T \approx 0.0022$ and we find that our apparatus must be at least four modules long to produce a change of ~ 0.01 in n. We designed our system to contain four quarter-wavelength modules. Because of the additional speakers at either end of the acoustic network to generate or absorb the traveling wave, though, we have a total of six acoustic drivers and approximately five quarter-wavelengths of duct.

For the design of the unit module from which the rest of the device is constructed, one must choose the frequency, the diameter of the duct, and the amplitude of the oscillations in the gas. In view of Eq. (4), one generally wishes to make the frequency as high as possible in order to make the device most compact in size. This has the advantages not only of making it easier to fit the machine in a room or enclosure but also of reducing the inventory of gas inside the machine during operation; the latter is particularly important when the feedstock is either expensive or hazardous. For a fixed total separation factor q_{tot}, though, the number of modules will remain the same no matter what the frequency is. The frequency is limited by either the surface smoothness of the duct or the properties of the drivers used. Any roughness in the inner surface of the duct must be smaller than the viscous and thermal penetration depths, which are themselves proportional to $1/\sqrt{\omega}$. Otherwise, the boundary layer may be destroyed by turbulence and would be difficult to characterize if it existed at all. For high efficiency in producing the sound wave, acoustic drivers must be operated close to their resonance frequency. However, there are constraints to the operating frequencies one can achieve with off-the-shelf components. For example, one may easily lower the resonance frequency of a mass-produced driver by adding mass

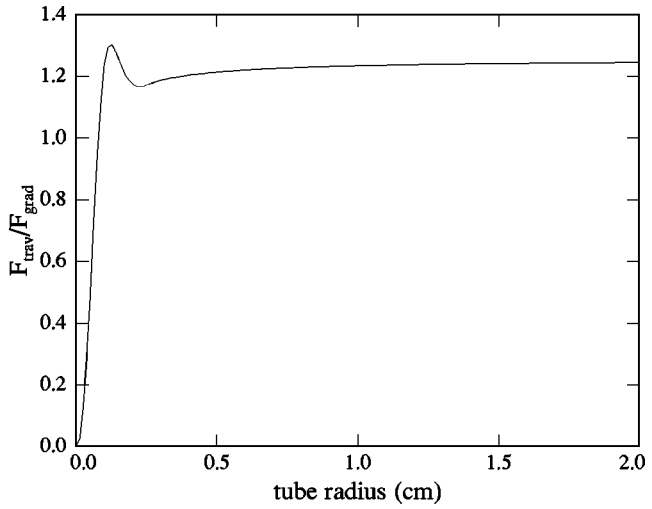

FIG. 2. A measure of the limit that the $|U_1|^2$ remixing imposes on the separation gradient in 80-kPa neon at 227 Hz. When diffusion can be neglected, little advantage is gained by reducing the radius of the duct.

of any type to the fixed moving mass of the actuator. Adding stiffness to raise the resonance frequency, however, is more difficult to achieve in practice: springs and bellows are produced in limited sizes and spring constants, and springs capable of large displacements suffer from surge at high frequencies.

Once the frequency is selected, one must choose a transverse dimension for the duct. We consider here specifically ducts of circular cross section, both because of the availability of such tubing in a variety of sizes and because it is relatively simple to calculate the separation in circular ducts. However, the considerations here will be essentially the same for ducts of arbitrary cross-sectional shape. Because the separation effect depends on the molecules diffusing into and out of the boundary layer, it is necessary for the duct's radius to be greater than the viscous and thermal penetration depths. As was shown by the experiments on He–Ar mixtures,[4] the phasing between p_1 and U_1 which yields the greatest separation is generally not that of a traveling wave, because generally $F_{\text{stand}} \neq 0$. For a given mixture, this optimal phasing also depends on the diameter of the tube. As will be shown in Sec. VIII, for our extended, modular systems the standing-wave component contributes little to the separation even across a single module. Therefore, one might consider reducing the tube diameter to the point at which the optimal phasing is that of a traveling wave. However, the limiting separation per module turns out not to be a maximum for this choice, because both F_{trav} and F_{grad} change with radius in such a way as to *reduce* the limiting concentration gradient as the tube diameter shrinks. Figure 2 demonstrates this for the case of the neon isotopes. The phasing is therefore not an important consideration in choosing the diameter of the duct.

One important factor in choosing the diameter arises instead from steady diffusion. If one can generate high enough velocity amplitudes in the duct that the second-order separation flux is much greater than the mole flux from steady diffusion when the concentration gradient reaches its maximum, then the concentration gradient is limited only by the frequency of operation. Also, it was seen in Ref. 5 that the limiting efficiency of a flow-through separator occurs (in the boundary layer limit) when $|U_1|$ is as high as possible before the onset of conditional turbulence, because the losses due to the remixing by steady diffusion are then insignificant. Thus, to have the highest gradient and best efficiency, one must keep the duct diameter narrow enough that the effect of diffusion is made small for values of $|U_1|$ below the onset of turbulence.

It is generally desirable to have the volume velocity as high as possible without breaking the acoustic drivers and without causing turbulence in a significant fraction of the duct. Also, in order to maintain agreement between the apparatus and its design calculations, one must limit the velocity such that the acoustic approximation may be applied: $\rho a|U_1|/A \approx |p_1| \ll p_m$, where p_m is the mean pressure.

Once the frequency, duct diameter, and maximum velocity are chosen, one can methodically develop the acoustic network. The first step is to design the elementary branched module, solving the equations of acoustics for the required impedance of the branch. For the quasitraveling wave system, a convenient module length is $\lambda/4$. The magnitude of the specific acoustic impedance $|z|$ in the middle of the module will differ slightly from ρa due to the attenuation in a finite-diameter duct; however, this deviation will be small except for tubes with radius of the order of the viscous penetration depth, and it can be corrected through small adjustments to the length of the module. Using the solution for the branch impedance and one's model for the acoustic drivers, one can then solve for the required voltage or displacement of the speaker and its phasing with respect to the pressure (or velocity) at the entrance to the module. The displacements of each branch speaker have the same amplitude, and their phases progress by $-90°$ from branch to neighboring branch along the direction of the traveling wave. From knowledge of the driver properties and of the pressure and velocity exiting the last module, one can design the active termination of the device, which can be considered as absorbing the traveling wave. It is convenient to choose the phasing of this last speaker to be the same as one of the quadrature phasings used in the rest of the series, but the displacement amplitude will generally be different from that of the other speakers. The greatest homogeneity in $|p_1|$ and $|U_1|$ is obtained by choosing the shortest module that makes the speaker phasing the same as that of the last branch speaker. Similarly, one must design the duct to the end speaker that acts as a source for the traveling wave. Again, it is convenient to choose one of the quadrature drive phasings, at the expense of having a third different displacement amplitude. For the greatest homogeneity of the amplitudes of pressure and velocity, one chooses this phase to lead the first branch by 90° and the shortest module for which this is obtained.

Although the separation occurs in the ducts, virtually the entire cost of the apparatus is due to the acoustic drivers. For these we use inexpensive stock parts: Radio Shack 4 1/2-in. RS-1052 woofers[17] and Servometer FC-16 nickel bellows (1-in. outside diameter, 10 convolutions).[18] In order to have a clean, hermetically sealed system with minimal dead volume, the speakers do not contact the neon sample directly.

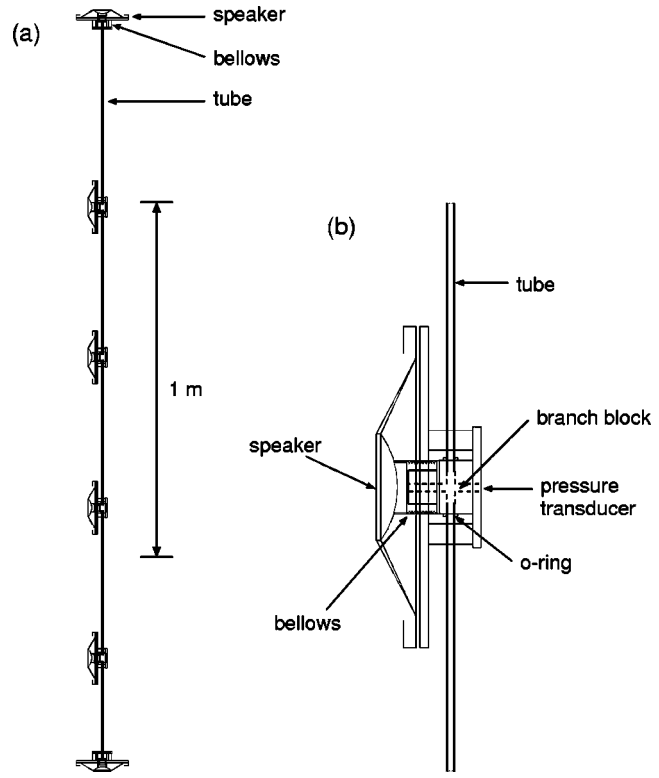

FIG. 3. A schematic of the traveling-wave apparatus. The salient features of the apparatus are shown in (a), while a detailed view of an acoustic driver is shown in (b). (Voice coils and magnet structures not shown.)

Instead, we use the speaker to drive the bellows, sealed on one end and soldered at the other end to a specially machined brass block which serves as either a tee (for side branches) or a straight-through connection (for ends) to the round stainless-steel stock tubing we use for ducts. The brass blocks provide a location for tapping in pressure sensors, thermocouples, and fill or sampling capillaries, and they are rigidly attached to the speakers' frames in order to support the ducts. The brass blocks also protrude into the bellows to eliminate some of their volume, and they present a flat surface as a stop to the sealed end of the bellows in order to prevent the bellows from collapsing beyond its elastic limit when the apparatus is evacuated. To preserve the modularity of the drivers, the tubing is sealed to the brass blocks with O-ring seals. Although the tees could have incorporated 90° bends to create a square coil without creating additional minor loss, we chose to make the system a straight array and mount it on a vertical rail. The linear arrangement made it easy to test different lengths of duct, because then one only needed to slide the speaker mounts along the rail to adjust their spacings. This design is depicted in Fig. 3.

Each bare speaker had a measured resonance frequency of approximately 80 Hz. Besides providing a closed boundary for the gas, the bellows increased the effective spring constant and resonance frequency for the composite driver. The sealed end of the bellows was connected to the speaker's dome by a thin fiberglass tube, which distributed the reaction force of the bellows in a ring far from the center of the dome. This was important, because the dome could easily collapse under a force applied at its center. The tube and the bellows combined to add about 3 g to the bare speaker's own moving mass of 9 g, partly offsetting the increased stiffness. Measurements of the drivers on the apparatus when sealed and filled with the 80-kPa neon used throughout this work showed the new resonance frequency to be about 157 Hz for all the drivers. Little increase in resonance frequency would have been obtained by shortening the fiberglass tube to reduce its mass further.

Although the resonance frequency for our drivers was 157 Hz, we chose to operate them at 227 Hz in the preferred, 90°-spaced mode. For this frequency at room temperature, the wavelength in the neon was 2 m, which for a λ-long apparatus was a convenient vertical clearance to work with in our lab. The duct consisted of stainless-steel tubing with a nominal inner diameter $2R=0.333$ cm, so that $R/\delta_\nu=6$ at 227 Hz. With this system, we were able to generate traveling waves at 227 Hz with $|p_1|$ up to 3350 Pa. This amplitude was sufficient for the concentration gradient to approach within 3% of its limiting value as imposed by the $|U_1|^2$ remixing term in the second-order mole flux.[4] At the highest amplitude, the Reynolds number was 770, based on the tube diameter $2R$ and the velocity $|U_1|/A$.

The quadrature drive signals were generated by two Hewlett-Packard 3325A synthesizers, synchronized by the same external clock in order to keep their relative phase locked. The quadrature signals were fed into a custom-built phase-shift box, consisting of six simple RC networks and isolation transformers, so that the relative phases of the six signals could be adjusted slightly. Outputs of each channel of the phase shifter were then fed to audio amplifiers, allowing us to adjust the voltage amplitude for each of the six speakers individually. The properties of the six acoustic drivers were not perfectly identical and our lumped-element model for the drivers was not perfect, so the ability to adjust both the drive amplitudes and phases was necessary for obtaining nearly ideal traveling waves in our network. The inadequacy of our speaker model had much more impact on the source and sink speakers at the ends of the network than on the side-branch speakers. There, we needed the flexibility to adjust their phases by as much as 20°, depending on the operating frequency. Corrections for the branch drivers, in contrast, were less than 5°. Even without more careful driver construction and analysis, a practical separator would not be strongly affected by such errors in drive voltage, so that the phase-shift network used here would be unnecessary: such an apparatus would consist of many more modules than our prototype does, so that local errors in the acoustics, as at the ends, would decay or be canceled locally and not extend far through the entire device.

For the purpose of creating the desired wave, there were five drive voltage amplitudes and five phases to be adjusted with respect to those of the first speaker, chosen to determine the overall amplitude and phase of the wave. To calculate how close a generated waveform was to our ideal traveling wave, the complex oscillating pressure was measured at each branch.[19] To establish the ideal settings for the complex drive voltages V_1, then, we inverted the 10×10 real matrix of derivative changes in p_1 with V_1 and calculated the matrix product of this inverse with the vector of deviations in p_1

from the ideal waveform. The result was the vector of changes in V_1 necessary to reach the ideal state. This process usually succeeded in producing a very close match to the ideal waveform within two iterations. Because the process of assembling the 10×10 matrix is labor intensive, it is fortunate that it will not be important in the operation of a longer apparatus, as noted above.

V. MEASURING THE NEON ISOTOPE CONCENTRATIONS

While in the He–Ar experiments of Ref. 4 the mole fractions were measured by the speed of sound in two small acoustic resonators, the changes in the speed of sound for the neon experiment would have been near the limit of resolution of that method. For example, a change $\Delta n=0.01$ in the concentration of ^{20}Ne would create a 0.05% change in the speed of sound, 16 times smaller than for a change of $\Delta n=0.01$ in the 50–50 He–Ar system. We therefore decided to measure the neon isotope concentrations directly with a quadrupole mass spectrometer.[20] Because the mass spectrometer requires a high vacuum (HV) system which is disrupted by the transients of opening valves to sample alternately each end of the apparatus, we chose to measure the concentration at one end only, obtaining the end-to-end concentration difference by doubling the difference between measured concentration and natural abundance. The acoustic-absorber end of the device was connected to the HV space of the mass spectrometer through a 5-μm glass capillary[21] cut to 5-cm length. This impedance allowed a mole flux of approximately 2.4×10^{-10} mol/s into the turbopumped HV space, which lowered the pressure in the acoustic network by approximately 1 kPa per day. Since each separation experiment lasted less than 1 day, the change in mean pressure of the apparatus had no noticeable impact on the data.

It was discovered early in our experimentation that the mass spectrometer itself was sensitive to temperature, and most of this sensitivity was associated with the control and detection electronics in spite of its built-in temperature compensation. Therefore, we housed the electronics and part of the mass spectrometer itself inside a sealed styrofoam box, the interior of which was cooled by a chilled water circuit. This thermal isolation held the temperature of the electronics constant to ±10 mK, more than two orders of magnitude better than our lab's climate-control system, making temperature drifts of the mass spectrometer's gains for different masses imperceptible in our data.

We also found it necessary to replace the HV system's original cold-trapped diffusion pump with a dry turbomolecular pump. While each of our experimental curves of concentration versus time took several hours to acquire, the liquid nitrogen level in the original diffusion pump's cold trap would necessarily fall over time, causing a gradual rise in the mass-22 signal until the trap was filled again. This spurious signal was directly correlated with a rise in the CO_2 signal, so it represented a double ionization of the CO_2 (mass 44) rather than a true neon signal. Filling the trap more frequently served only to produce more jumps in the apparent concentration of ^{22}Ne. Thus, the diffusion pump was unacceptable. (We could not use an independent Bayard–Alpert ionization gauge to measure total pressure, because the thoriated-iridium filament produced prodigious quantities of CO_2 which also caused a large, noisy background[22] to the partial pressure measurement of ^{22}Ne.)

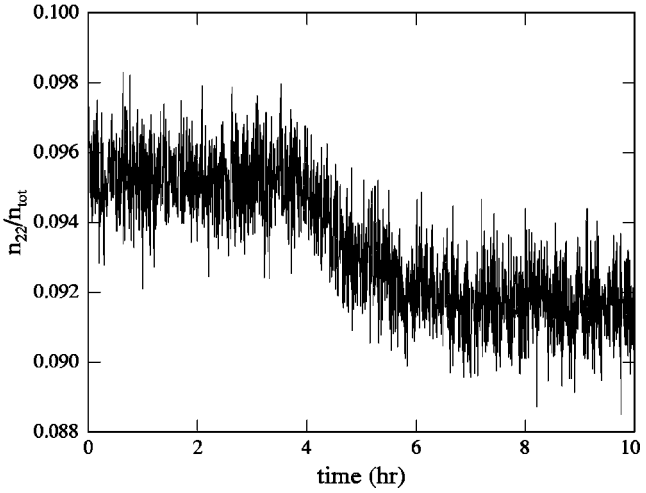

FIG. 4. Raw data from a typical separation experiment. This data set was taken for a traveling wave with $|p_1|=1.1$ kPa and a frequency of 227 Hz. The neon isotopes are at their natural abundances before the sound wave is applied at $t_0\approx4$ h.

Unlike the previous experiments in He–Ar, these experiments allowed continuous measurement of the mole fractions, without stopping the acoustic wave in the separation duct. Figure 4 shows a typical curve for the mole fraction of the ^{22}Ne as a function of time.[23] Although the separation effect is clearly visible, the signal appears noisy. This is partly because of the vertical offset of the graph; the fractional standard deviation is only 1%.

The output of the mass spectrometer is given in terms of the partial pressure for each mass number, and we examined the noise in the recorded partial pressures for several different values of partial pressure and for several different mass numbers. In general we found that the standard deviations were always approximately 1%, regardless of pressure or mass number. This suggests that virtually all of the noise is caused by the electronics and that the shot noise, proportional to $\sqrt{p_i}$, was a negligibly small component of the total noise observed. This is consistent with the fact that this mass spectrometer uses a logarithmic amplifier to span the seven orders of magnitude in partial pressure that it is capable of measuring, rather than by having an adjustable gain amplifier. In the logarithmic amplifier, large input currents are compressed to fit the range of the gain stage, while the gain of the final amplifier is held constant. This results in a constant fractional noise, instead of a fractional noise that is inversely proportional to the input signal as it would be in a detector with variable gain. Although some resolution would be lost even for a low-noise detector of variable gain by the need to digitize the amplifier's analog output signal, the fluctuations in our mass spectrometer were about an order of magnitude greater than the errors from digitization. Thus, much greater signal-to-noise ratio should be possible with other mass spectrometers.

Because of the low signal-to-noise ratio, it was especially important in analyzing the data to constrain the fits as much as possible and thereby reduce their uncertainty. Before each experiment, the mass spectrometer was allowed to run long enough to ensure that it had reached equilibrium, the equilibration time depending on whether the mass spectrometer was just started, was degassed, or had its power cycled momentarily to reboot the control electronics. Baseline partial pressures of masses 20, 22, 40, and 44 were then collected, so that the doubly ionized mass-40 and mass-44 backgrounds could be subtracted from the mass-20 and mass-22 signals, and the starting concentration determined accurately from its average over time. The sound wave was then applied, the start time t_0 was recorded, and the sound was allowed to separate the gases until the mole fraction of ^{22}Ne was not measurably changing. The uncertainty in start times is 20–40 s, determined by the interval between mass spectrometer measurements and by a time lag for the first measurement, originating in the mass spectrometer control software.

In spite of the presence of six reservoirs along the length of the duct (instead of only two as in the He–Ar experiments), the batch-mode limiting can be modeled by an exponential decay to the limiting gradient with a single time constant. Therefore, the data after t_0 were fit to an exponential with only the magnitude and the time constant of the exponential term as free parameters. Because of the quality of the exponential fits in comparison to linear fits near t_0, the time constant was used to determine the initial slope of the separation for comparison with the theory. Often, at the end of an experiment, the valve from the capillary leak to the mass spectrometer's HV chamber was closed, and the residual signals from masses 20, 22, 40, and 44 were remeasured in order to confirm the background pressures of cracked hydrocarbons.

VI. EXPERIMENTAL RESULTS

The first set of experiments was carried out to demonstrate the agreement between the data and theory for this multiple-driver thermoacoustic separator. The difference in steady-state concentration Δn of the ^{22}Ne between one end of the duct and the other was measured as a function of the pressure amplitude $|p_1|$ for a quasitraveling wave at 227 Hz. The results are shown in Fig. 5 and compared with our calculations. These calculations use the measured complex p_1 at each speaker location to calculate the x dependences of p_1, U_1, and $(dn/dx)_{\mathrm{lim}}$ along the duct with the "circular-tube" algorithm of Ref. 4. The concentration difference is then calculated from a numerical integration of $(dn/dx)_{\mathrm{lim}}$ along the duct. Agreement is good, considering the variation in quoted values of the thermal diffusion coefficient $\alpha_T = k_T/n(1-n)$ for neon[16] at room temperature. There is no measurable reduction in the measured separation at the highest $|p_1|$, where turbulent mixing might occur. No turbulent mixing is expected along most of the duct length, because the highest Reynolds number attained in these data is 772, and the duct radius is 6 times δ_ν, putting the motion in the weakly turbulent regime where no significant perturbation of the boundary-layer physics is expected.[24,25] Nevertheless, the result suggests that any turbulence or jetting at the branches, where the acoustic network has tees, does not expand dramatically with the amplitude of sound to adversely affect the separation.

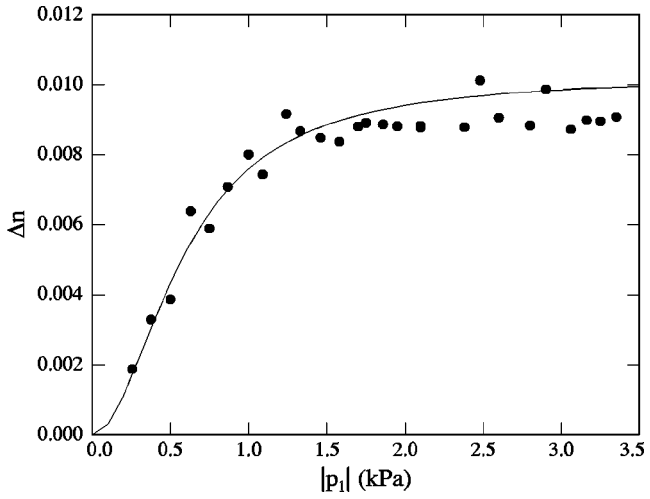

FIG. 5. Total difference in steady-state concentration of ^{22}Ne between ends of the apparatus. Data are for 227 Hz in a duct of total length 2.11 m. Points represent measured values and the curve is the result of a calculation with no adjustable parameters.

Using the time constants from the exponential fits, one can compare the initial mole flux in the apparatus to Eq. (54) of Ref. 4 when $dn/dx=0$. To extract the initial mole flux from a data set, it is tempting to write simply

$$\dot{N}|_0 = \frac{1}{\tau}\frac{\Delta n_{\mathrm{lim}}}{2}\eta V_{\mathrm{res}}, \tag{5}$$

where Δn_{lim} is the total change in concentration across the apparatus in steady-state, τ is the time constant from the exponential fit, η is the molar number density, and V_{res} is the volume of the reservoir at the end of the apparatus where the concentration is measured. However, that identity assumes that all of the volume of the device is in the end reservoirs. For our apparatus, each tubing segment has a volume approximately equal to that of each driver, so most of the volume is in the duct and branch drivers. Therefore, one must add to the volume of the end reservoir the volumes of the duct and branches, weighted by their change in concentration when a finite gradient is established. The end reservoir, like all the acoustic drivers in our system, has a volume of approximately 3.6 cm^3, but the additional, effective volume of the apparatus from the midpoint (where the concentration remains constant) is approximately 7.5 cm^3. The results are plotted against Eq. (54) of Ref. 4 in Fig. 6, where the agreement is seen to be excellent.

VII. SEEKING EFFECTS OF TURBULENCE

Both high mole flux and high concentration gradient demand high acoustic amplitude, but turbulence prevents an arbitrary increase in amplitude. No evidence of turbulence was observed in these measurements, but this section presents a brief exploration of some of the relevant issues and parameter space.

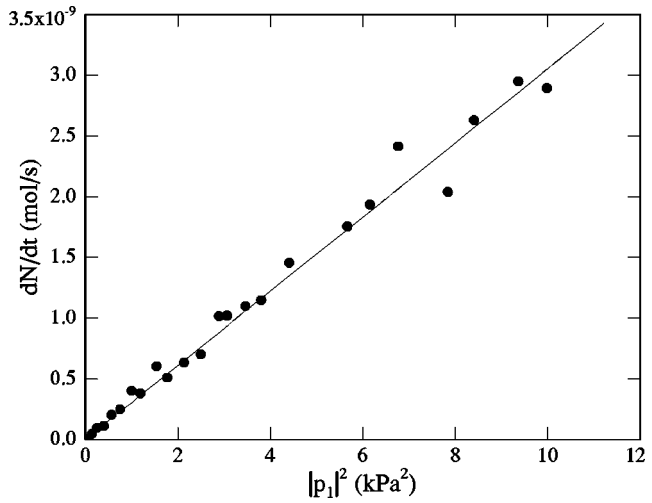

FIG. 6. Theory and data for mole flux of separation at $t=0$, when the components are well mixed, for a frequency of 227 Hz and a duct radius of 1.66 mm.

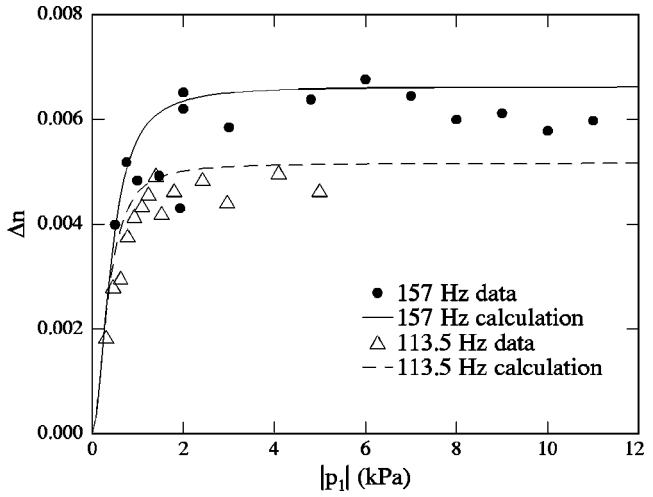

FIG. 7. No evidence of a transition from laminar flow to weak turbulence is seen in the steady-state concentration difference at either 113.5 or 157 Hz.

In the separation duct itself near the necessarily disturbed geometry of each branch, the flow field of the gas is turbulent. This can affect the separation in two ways. First, the turbulence causes a pressure drop near the branch—the ''minor loss''—so that the branch speaker will have to be driven harder than calculations assuming laminar flow would predict. Second, the turbulence destroys the boundary layer and remixes the gas constituents in the vicinity of the branch. Since this remixing takes place very close to the location where the separative effect should be strongest, and the turbulently disturbed region probably grows with increasing amplitude, the true separation across the duct could be significantly lower than the laminar theory predicts.

Turbulence may hinder operation of the nearly traveling-wave configuration in a more spatially extended way as well. If, for a fixed operating frequency of the apparatus, the duct is narrower in diameter than approximately 5 times the viscous penetration depth δ_ν, then for low-amplitude operation the oscillating motion of the gas will be laminar.[24,26,27] At velocity amplitudes high enough to make the Reynolds number 1000–2000, though, the oscillating flow in the duct can cross into the conditionally turbulent regime, destroying the boundary layer wherever such high velocities occur. This will eliminate the separative effect from the beginning of each module out to the point along the duct at which the local velocities are low enough for the gas motion to be laminar. For traveling-wave systems in which the module length is less than $\lambda/2$, the velocity amplitude is relatively constant so that the entire module will become turbulent at a pressure amplitude only slightly larger than that at which turbulence first appears. This crossover to conditional turbulence should also occur when the duct's radius is larger than $\sim 5\delta_\nu$, but such systems will be in the weakly turbulent regime at low amplitudes and will cross over to conditional turbulence only at significantly higher amplitudes of velocity compared to the laminar case.

To experimentally explore the possibility of turbulence destroying thermoacoustic separation, we studied the performance of the apparatus at two other frequencies, 113.5 and 157 Hz. For these frequencies, we chose to abandon the preferred $-90°$ phase-shift condition between adjacent branches, instead using our phase-shift networks to create the appropriate phasing that produced traveling waves. This was done in order to avoid changing the duct lengths. At these lower frequencies, Reynolds numbers up to 2500 were reached, but operating conditions were always close to the region of crossover from laminar to weakly turbulent flow.[24] At the highest amplitudes $|p_1|/p_m > 1/10$, so that the validity of the acoustic approximation used in calculating the separation is questionable. Nevertheless, all these lower-frequency data (Fig. 7) show no abrupt decline in the separation at high amplitudes. Although these data do not rule out effects of turbulence, they suggest that the penalty in separation for having weakly turbulent flow is small. Also, the duct sizes for which a transition to conditional turbulence would be easiest to achieve are so small, of order $R/\delta_\nu < 3$, that the separation would be disadvantaged by the effect shown in Fig. 2.

VIII. THE HIGH-IMPEDANCE APPROACH

In order to mitigate the sources of turbulent mixing, it may be useful to consider configurations of concatenated branched modules with a specific acoustic impedance higher than ρa, at least near the middle of each module. If the acoustic impedance is increased, the volume velocity—and, therefore, the Reynolds number—will be lower for the same value of acoustic power. From Eq. (54) in Ref. 4, one also sees that increasing $|Z| = |p_1|/|U_1|$ as the product $|p_1||U_1|$ is held fixed can lead to larger values of the concentration gradient because it decreases the relative importance of the $|U_1|^2$ remixing process compared to the mole flux of separation. Thus, increasing $|Z|$ seems like a promising way to improve the performance of thermoacoustic separation. Although this is true, one does not have as much flexibility in choosing $Z(x)$ as one might expect.

Ideally, one would like to adjust $|Z|$ to be as high as possible, and to choose the phase $\theta = \arg(Z)$ to be that which would produce the largest concentration gradient, i.e., $\theta = \tan^{-1}(F_{\text{stand}}/F_{\text{trav}})$. To do this, there are two parameters of

each module one may adjust: the module's length L and the temporal phase lag $\Delta\phi$ between p_1 at the beginning and end of the module. (Note that the volume velocity must share this phase lag; otherwise, the phase θ between p_1 and U_1 would change incrementally at the beginning of each successive module, eventually reversing the direction of the mole fluxes of the components and defeating the purpose of the concatenation of modules.)

In order to relate the magnitude and phase of the acoustic impedance in the middle of the duct to L and $\Delta\phi$, we need the solution to the coupled first-order equations for $p_1(x)$ and $U_1(x)$ in the duct.[28] Applying the boundary condition for the duct segment $p_{\text{out}}=p_{\text{in}}e^{\imath\Delta\phi}$ in the equation for $p_1(x)$, one finds that

$$p_{\text{in}}=\frac{-\imath Z_0 U_{\text{in}}\sin kL}{e^{\imath\Delta\phi}-\cos kL}, \tag{6}$$

$$p_1(x)=-\imath Z_0 U_{\text{in}}\left[\frac{\sin kL\cos kx}{e^{\imath\Delta\phi}-\cos kL}+\sin kx\right], \tag{7}$$

$$U_1(x)=U_{\text{in}}\left[\cos kx-\frac{\sin kL\sin kx}{e^{\imath\Delta\phi}-\cos kL}\right], \tag{9}$$

where k is the complex wave number, $Z_0=\omega\rho_m/kA(1-f_\nu)$ is the acoustic impedance of a traveling wave in the duct of area A, and f_ν is the complex correction for viscosity. In the middle of the duct we set $x=L/2$ to find

$$z(x=L/2)\equiv z_{\text{mid}}=-z_0\tan(kL/2)\cot(\Delta\phi/2), \tag{10}$$

where the $z_i=Ap_1/U_1$ are specific acoustic impedances. Because both z_0 and k are generally complex, z_{mid} typically has a complex value. From this expression, we see that changing the phase shift $\Delta\phi$ across the duct will alter the magnitude of the impedance in the middle of the duct but not the phase. Changing the length of the duct, however, alters both the magnitude and the phase of the impedance in the middle. Nevertheless, it is not possible to arbitrarily choose both $|z|$ and θ: for example, no combination of L and $\Delta\phi$ allows one to obtain $\theta\geqslant 0$ in the middle of the tube. For ducts wide enough to be well represented by calculations in the boundary-layer limit, $F_{\text{stand}}/F_{\text{trav}}>0$ so that it is not possible to make the phasing at the center of the tube optimal.[2,4] This is not an important restriction in choosing the radius of the duct, because both analytical and numerical studies show that the standing-wave component never contributes significantly to the separation across a module.

As for the nearly traveling-wave system described above, $|p_1|$, $|U_1|$, θ, and the limiting concentration gradient will vary along each module of a configuration designed to provide $|z|>\rho a$. Alterations of L and $\Delta\phi$ to generate these higher-z configurations effectively do so by adding in a traveling-wave component opposed to the direction of the wave in the $z\approx\rho a$ system. The velocity of this added wave attenuates as it travels in the opposite direction from each branch, ensuring that the velocity has its minimum somewhere away from the ends of the module. This tends to push the maximum of $|z|$ and of the concentration gradient away from the ends of the module as desired.

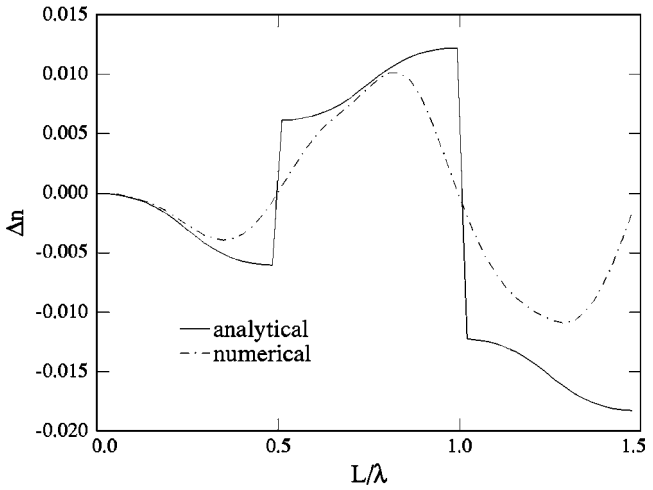

FIG. 8. The separation Δn per module, as a function of module length L, calculated for the inviscid analytical model (solid curve) and for the full numerical model (dash-dot curve) in the boundary-layer limit. The phasing across the branch is fixed at $\Delta\phi=-90°$.

There is a large parameter space to analyze in determining what is the best higher-z configuration to use in a separation device. One must first decide whether it is most important that the device be as short as possible, and thus to generate the highest gradient dn/dx, or whether it is more important to maximize the separation Δn per module of the acoustic network. Here, we make the latter choice, because the number of active branches is probably most important in terms of a separator's capital cost. One may then look for the combination of L and $\Delta\phi$ that provides the highest Δn.

We have studied this problem both numerically and with a simplified analytical calculation.[29] Plots of both numerical and analytical calculations of Δn versus L with $\Delta\phi$ held fixed at $-90°$ are shown in Fig. 8. For module length $L>\lambda/4$ the curves begin to diverge (although they remain similar qualitatively), with the analytical calculation predicting higher Δn because it neglects viscosity and thermal conductivity in the wave number. For $L>\lambda/2$, dn/dx and $\dot{N}_2$ vary spatially along the tube in a complicated way, possibly yielding locations where there is a bottleneck in the separation flux. If the parameter space is therefore limited to $L\leqslant\lambda/2$, one finds that Δn will be maximized as $L\to\lambda/2$ and $\phi\to 0$. The resulting Δn in that limit is, for the analytical calculation, a factor of 2 higher than for the preferred, traveling-wave system we considered in the previous sections.

The actual improvement in Δn that can be achieved will be smaller than this, because it is dangerous to design L too close to $\lambda/2$. For L near $\lambda/2$, a small decrease in the speed of sound (arising from, say, a change in temperature or gas composition) would cause L to become greater than the intended $\lambda/2$. This would lead to a change in both magnitude and sign for the separation in that module, possibly defeating the purpose of the device.

In order to test our understanding of the high-z approach, we measured the separation as a function of $|p_1|$ for $|z_{\text{mid}}|\approx 2.5\,\rho a$ at 227 Hz. This configuration was achieved by keeping all the duct lengths the same but phasing adjacent

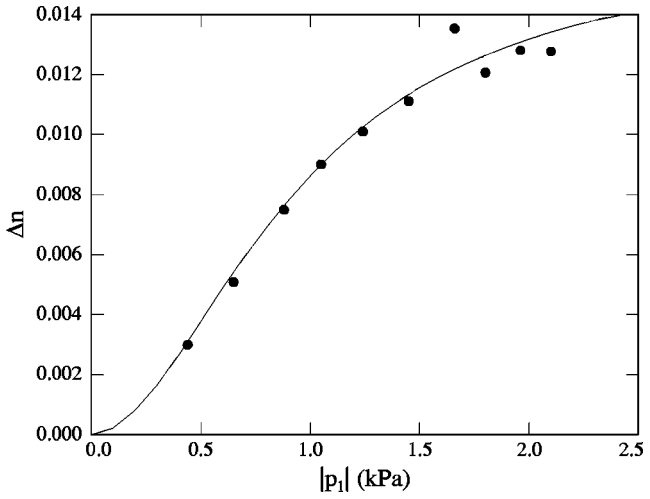

FIG. 9. The difference in steady-state concentration of ^{22}Ne across the apparatus for $|z_{\mathrm{mid}}| \approx 2.5\ \rho a$ in the middle of each module.

branch speakers $-45°$ apart in time, instead of the $-90°$ spacing of the nearly traveling-wave system. The data from this study are shown in Fig. 9, where agreement with calculations is again seen to be quite good. As $|p_1|$ is increased, calculations show that Δn should approach a limiting value of ~ 0.015, or approximately 50% higher than for the nearly traveling-wave configuration.

IX. CONCLUSIONS

This paper shows that thermoacoustic mixture separation, discovered only in the past decade, is extensible to arbitrarily high purities by maintaining a quasitraveling wave through an arbitrarily large number of wavelengths of sound, using a periodic, modular series assembly of tubes and drivers. In the proof-of-principle ^{22}Ne enrichment described here, an enrichment from the natural abundance of 0.092 to 0.097 was achieved at one end of the apparatus with 5 quarter-wavelength modules using $|z| \approx \rho a$. From the point where the mixture consisted of its natural abundances, this enrichment required approximately 2.5 modules; to obtain 0.90 ^{22}Ne from a reservoir of natural abundance would require only 148 modules, and to obtain 0.99 ^{22}Ne would require only 232 modules.

A variant of the method, using a spatially periodic wave with regions of enhanced acoustic impedance, promises modest, factor-of-2 reduction in the number of modules required for a given purity. Other interesting, quantitative physics issues that could lead to modest changes in expected performance include the transition to turbulence, which was not encountered in the present measurements, and the remixing effect of streaming.[4]

Further analysis and experimentation are also required to develop practical steady-flow separators in which a nonzero time-independent mole flux and nonzero concentration gradient are present simultaneously, and to learn whether single devices can achieve high throughput by use of stack-like parallel arrays of channels without counterflowing streaming in different channels causing unacceptable remixing.

The modular apparatus can be coiled, with either curved or straight tubular modules, to form a compact system, one in which each same-phase set of periodically arrayed acoustic drivers can share common electromechanical transduction hardware if the length of each turn of the coil equals one wavelength of sound in the gas. However, to fully enjoy the low-cost, high-reliability promise of thermoacoustics, the thousands of joints that would be present in a straightforward multiplication of our 5 modules should be eliminated. Perhaps future work will demonstrate a good way to drive a peristaltic wave in the cross-sectional area of a long, coiled, flexible-walled tube without joints.

ACKNOWLEDGMENTS

The authors are grateful to Mark Hollander for his assistance in improving our vacuum system. We also thank Scott Backhaus for inducing us to consider the effect of standing-wave components. This work was supported by the Office of Basic Energy Sciences in the U.S. Department of Energy's Office of Science.

APPENDIX: RESULTS FROM EARLIER WORK

Useful results and definitions from Refs. 2, 4, and 5 are collected here, expressed in terms of mole fractions and mole fluxes. For a discussion in terms of mass fractions and mass fluxes, see those references.

The separation flux to second order is given by combining Eqs. (41), (44), and (56) of Ref. 4

$$\dot{N}_H = \frac{\delta_\kappa}{4r_h}\frac{\gamma-1}{\gamma}\frac{k_T}{R_{\mathrm{univ}}T_m}|p_1||U_1|[F_{\mathrm{trav}}\cos\theta + F_{\mathrm{stand}}\sin\theta] + \frac{\delta_\kappa}{4r_h}\frac{\rho_m|U_1|^2}{\omega A M_{\mathrm{avg}}}F_{\mathrm{grad}}\frac{dn_H}{dx} - NAD_{12}\frac{dn_H}{dx}. \tag{A1}$$

In the boundary-layer approximation, the Fs are given by

$$F_{\mathrm{trav}} = \frac{\sigma\sqrt{\sigma L} - \sqrt{\sigma} - \sigma\sqrt{L}(\delta_{\kappa D}/\delta_\kappa + \delta_{D\kappa}/\delta_\kappa)}{(1+\sqrt{L})[(1+\sigma)(1+\sigma L)+\varepsilon\sigma]}, \tag{A2}$$

$$F_{\mathrm{stand}} = \frac{-\sigma\sqrt{\sigma L} + \sqrt{\sigma} - \sigma\sqrt{L}(\delta_{\kappa D}/\delta_\kappa + \delta_{D\kappa}/\delta_\kappa)}{(1+\sqrt{L})[(1+\sigma)(1+\sigma L)+\varepsilon\sigma]}, \tag{A3}$$

$$F_{\text{grad}}=\frac{\sqrt{\sigma}L(1-\sigma^2)(1+\sqrt{L})+\varepsilon\sqrt{\sigma}(\sqrt{L}-1)+[(\sigma^2-1)L+\varepsilon\sigma\sqrt{L}](\delta_{\kappa D}/\delta_\kappa+\delta_{D\kappa}/\delta_\kappa)}{(1+\sqrt{L})[(1+\sigma)(1+\sigma L)+\varepsilon\sigma][(1-\sigma)(1-\sigma L)-\varepsilon\sigma]/\sigma} \tag{A4}$$

with

$$\delta_{\kappa D}^2=\tfrac{1}{2}\delta_\kappa^2[1+(1+\varepsilon)/L+\sqrt{[1+(1+\varepsilon)/L]^2-4/L}], \tag{A5}$$

$$\delta_{D\kappa}^2=\tfrac{1}{2}\delta_\kappa^2[1+(1+\varepsilon)/L-\sqrt{[1+(1+\varepsilon)/L]^2-4/L}], \tag{A6}$$

$$\varepsilon=\frac{\gamma-1}{\gamma}\frac{k_T^2}{n_H(1-n_H)}. \tag{A7}$$

The more complicated Bessel-function forms of the Fs, accurate for circular tubes of arbitrary radius, are described (but not displayed) in Ref. 4.

Equation (A1) describes the mole flux for any value of the concentration gradient dn_H/dx. Our experiments typically start with $dn_H/dx=0$ and proceed toward the limiting state where $\dot{N}_H=0$. In this limiting state, the concentration gradient is given by Eq. (25) of Ref. 5

$$\left(\frac{dn_H}{dx}\right)_{\text{lim}}=\frac{(F_{\text{trav}}\cos\theta+F_{\text{stand}}\sin\theta)(\gamma-1)k_T|p_1||U_1|/A\gamma p_m}{4D_{12}r_h/\delta_\kappa-F_{\text{grad}}|U_1|^2/A^2\omega}. \tag{A8}$$

TABLE I. Variables used in the Appendix. Units are MKS.

A	area of duct (m^2)
c_p	isobaric heat capacity per unit mass (J/kg·K)
D_{12}	binary mass diffusion coefficient (m^2/s)
$\dot{E}$	acoustic power (W)
k	thermal conductivity (W/m·K)
k_T	thermal diffusion ratio
L	$k/\rho_m c_p D_{12}$
M_{avg}	mixture average molar mass (kg/mol)
$\dot{N}_H$	mole flux of heavy component (mol/s)
N	mixture molar density (mol/m^3)
n_H	mole fraction of heavy component
p_m	mean pressure (Pa)
$\|p_1\|$	amplitude of oscillating pressure (Pa)
R_{univ}	universal gas constant (J/mol·K)
r_h	hydraulic radius of duct (m), A/Π
T_m	mean temperature (K)
$\|U_1\|$	amplitude of oscillating volume velocity (m^3/s)
x	coordinate along sound-propagation direction (m)
γ	ratio of isobaric to isochoric specific heats
δ_ν	viscous penetration depth (m), $\sqrt{2\mu/\omega\rho_m}$
δ_κ	thermal penetration depth (m), $\sqrt{2k/\omega\rho_m c_p}$
δ_D	mass-diffusion penetration depth (m), $\sqrt{2D_{12}/\omega}$
θ	phase angle by which p_1 leads U_1
μ	dynamic viscosity (kg/m·s)
Π	duct perimeter (m)
ρ_m	mean density (kg/m^3)
σ	Prandtl number, $\mu c_p/k$
ω	angular frequency (s^{-1})

Acoustic power per unit length consumed by the mixture-separation process is given by Eqs. (19)–(22) in Ref. 5, but an excellent approximation is that given for a pure gas by Eq. (5.10) in Ref. 25. In the boundary-layer approximation, the latter becomes

$$\frac{d\dot{E}_2}{dx}=-\frac{\Pi\delta_\nu}{4}\rho_m\left|\frac{U_1}{A}\right|^2\omega-\frac{\Pi\delta_\kappa}{4}\frac{|p_1|^2}{\gamma p_m}(\gamma-1)\omega. \tag{A9}$$

The thermodynamic efficiency of thermoacoustic mixture separation is the ratio of the rate at which the Gibbs free energy of the mixture increases to the rate of acoustic power consumed. Reference 5 shows that this efficiency is highest when dn_H/dx is half of the limiting value given in Eq. (A8). Using this value of concentration gradient and several other simplifying assumptions yields the upper bound on the efficiency given by Eq. (36) in Ref. 5

$$\eta_{\text{best}}\approx\frac{\varepsilon}{4}\frac{2(1+\sqrt{\sigma L})}{\sqrt{L}(1+\sqrt{L})^2(1+\sigma)}. \tag{A10}$$

Other variables are defined in Table I.

[1] *Encyclopedia of Separation Technology*, edited by D. M. Ruthven (Wiley, New York, 1997).

[2] G. W. Swift and P. S. Spoor, "Thermal diffusion and mixture separation in the acoustic boundary layer," J. Acoust. Soc. Am. **106**, 1794–1800 (1999); **107**, 2229(E) (2000); **109**, 1261(E) (2001).

[3] P. S. Spoor and G. W. Swift, "Thermoacoustic separation of a He–Ar mixture," Phys. Rev. Lett. **85**, 1646–1649 (2000).

[4] D. A. Geller and G. W. Swift, "Saturation of thermoacoustic mixture separation," J. Acoust. Soc. Am. **111**, 1675–1684 (2002).

[5] D. A. Geller and G. W. Swift, "Thermodynamic efficiency of thermoacoustic mixture separation," J. Acoust. Soc. Am. **112**, 504–510 (2002).

[6] D. Geller, G. Swift, and S. Backhaus, "Method and apparatus for separating mixtures of gases using an acoustic wave," U.S. Serial No. 10/238,250, filed with the U.S. Patent Office on 10 September 2002; allowed 13 January 2004.

[7] D. Massignon in *Topics in Applied Physics: Uranium Enrichment*, Vol. 35, edited by S. Villani (Springer, New York, 1979), pp. 55–56.

[8] K. Clusius and G. Dickel, "Neues Verfahren zur Gasentmischung und Isotopentrennung," Naturwissenschaften **26**, 546(L) (1938).

[9] See *Handbook of Chemistry and Physics, 64th ed.* (CRC Press, Boca Raton, FL. 1984), p. B-235. Besides the two main isotopes, ^{21}Ne is present at a concentration of 0.27%.

[10] As a measure of the difficulty in separating the neon isotopes compared to He–Ar mixtures, the 157-Hz neon data described below can be compared with data we obtained at the same frequency after filling this apparatus with a sample mixture of 55–45 He–Ar, which has the same sound speed as neon. In He–Ar, with a pressure amplitude of 2650 Pa, the apparatus produced concentration differences $\Delta n\sim 0.4$ across the duct—more than 50 times larger than the Δn obtained with 91–9 ^{20}Ne–^{22}Ne mixtures at the same operating frequency.

[11] Acousticians use the term "volume velocity" for what engineers call "volume flow rate."

[12] C. C. Lawrenson, L. Dwynn Lafleur, and F. Douglas Shields, "The solution for the propagation of sound in a toroidal waveguide with driven walls (the acoustitron)," J. Acoust. Soc. Am. **103**, 1253–1260 (1998).

[13] The thermal diffusion ratio is in general nearly proportional to $n(1-n)$. He–Ar mixtures, for example, have $k_T=0.38n^{0.8}(1-n)^{1.2}$, based on fits to the data of Atkins *et al.* [Proc. R. Soc. London, Ser. A **172**, 142–158

(1939)]. For this reason, the literature often defines another parameter $\alpha_T \equiv k_T/n(1-n)$, called the thermal diffusion coefficient. The thermal diffusion coefficient is a function of temperature but has only a weak dependence on the concentrations.
[14] Stelio Villani, *Isotope Separation* (American Nuclear Society, LaGrange Park, IL, 1976).
[15] H. London, *Separation of Isotopes* (Newnes, London, 1961).
[16] S. Weissman, "Self diffusion coefficient of neon," Phys. Fluids **16**, 1425–1428 (1973).
[17] RadioShack Corp., 300 West Third Street, Suite 1400, Fort Worth, TX 76102. http://www.radioshack.com
[18] Servometer, 501 Little Falls Road, Cedar Grove, NJ 07009; http://www.servometer.com
[19] 8510B pressure transducer, Endevco, San Juan Capistrano, CA; http://www.endevco.com; SR830 lock-in amplifier, Stanford Research Systems, Sunnyvale, CA; http://www.srsys.com
[20] RGA100, Sanford Research Systems, Sunnyvale, CA, http://www.srsys.com
[21] Polymicro Technologies, LLC, 18019 N. 25th Ave., Phoenix, AZ 85023; http://www.polymicro.com
[22] J. F. O'Hanlon, *A User's Guide to Vacuum Technology*, 2nd ed. (Wiley, New York, 1989), p. 141.
[23] The reader may notice that the equilibrium concentration in Fig. 4 before separation appears to be 9.53% rather than the 9.22% quoted in Ref. 9. We attribute this to an error in the calibration of the mass spectrometer.
[24] M. Ohmi, M. Iguchi, K. Kakehashi, and T. Masuda, "Transition to turbulence and velocity distribution in an oscillating pipe flow," Bull. JSME **25**, 356–371 (1982).
[25] G. W. Swift, *Thermoacoustics: A Unifying Perspective for some Engines and Refrigerators* (Acoustical Society of America, Melville, NY, 2002).
[26] U. H. Kurzweg, E. R. Lindgren, and B. Lothrop, "Onset of turbulence in oscillating flow at low Womersley number," Phys. Fluids A **1**, 1972–1975 (1989).
[27] M. Hino, M. Sawamoto, and S. Takasu, "Experiments on transition to turbulence in an oscillatory pipe flow," J. Fluid Mech. **75**, 193–207 (1976).
[28] Reference 25, Eqs. (4.54) and (4.70) with $dT_m/dx = 0$.
[29] The analytical calculation of Δn across a module of arbitrary L and $\Delta\phi$ becomes tractable when turbulence and steady diffusion are ignored and the wave number is taken to be real.